Electronic Supplementary Material (ESI) for RSC Advances.


# Supporting Information

## Synthesis of Disordered Mesoporous Silica Loaded with Ultrasmall Sized CuO Nanoparticles Based on Alkali-free Strategy and Its Excellent Catalytic Performance on Reduction of Organic Dye

Li Jiaze, Xu Linxu*, Chen Feiyong, Yang Zhigang, Shen Xue, Wang Jin, Xu Sisi and Song Yang*

*Institute of Resources and Environment Innovation，Shang Dong Jianzhu University，Jinan, Shandong, People's Republic of China*

E-mail: *xulinxu20@sdjzu.edu.cn; songyang20@sdjzu.edu.cn*

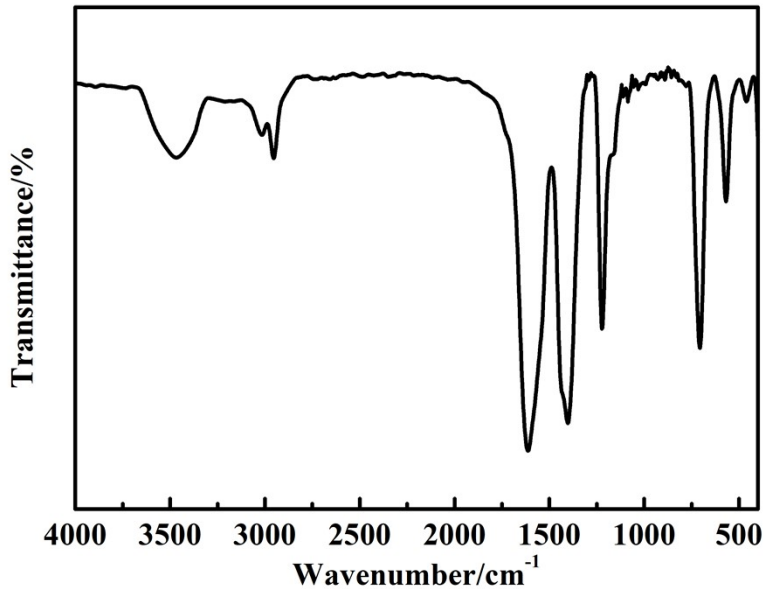


Figure. S1 the FT-IR spectrum of CuBA

Figure S1 shows the FT-IR spectrum of synthesized CuBA. The two bands appearing at 3018 and 2954 $cm^{-1}$ are ascribed to the antisymmetric stretching vibration and symmetric stretching vibration of methylene. Three strong peaks are shown at 1613, 1407 and 707 $cm^{-1}$, which can be assigned to the antisymmetric stretching vibration, symmetric stretching vibration and deformation vibration of the carboxylate groups, respectively. The peaks at 1216 $cm^{-1}$ and 570 $cm^{-1}$ are the the out-of-plane vibration of methylene and the stretching vibration of C–Br groups, respectively. As a result, we believe that CuBA has been successfully obtained.

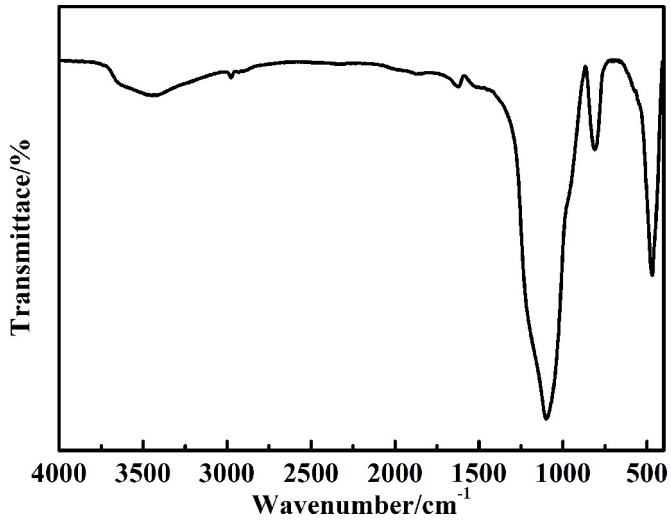


Figure S2 the FT-IR spectrum of CuO@m$SiO_2$ material

Figure S2 shows the FT-IR spectrum of CuO@m$SiO_2$ material, After the thermal treatment of the organic- inorganic hybrid CuBA@$SiO_2$ material, all alkyl chains were decomposed. The peaks presenting at 1100 and 802 $cm^{-1}$ are the antisymmetric stretching vibration and symmetric stretching vibration of amorphous Si-O-Si, which can be explained that organosilicone transformed into amorphous silica materials.

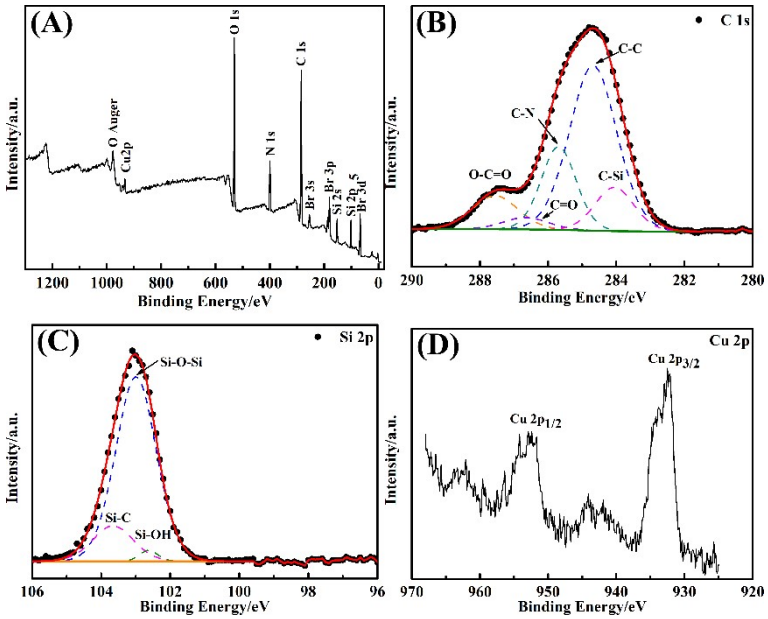


Figure S3 XPS spectra of the obtained CuBA@$SiO_2$ naoncomposites

Figure S3 shows the typical XPS spectra of the obtained CuBA@$SiO_2$ naoncomposites. The full scanned spectrum shown in Figure S3(A) demonstrates that Br, Si, C, N, O and Cu elements exist in CuBA@$SiO_2$ nanocomposites. Figure S3(B) shows the spectrum of C 1s was fitted by multiple Gaussians. The C 1s can be deconvoluted into five peaks with binding energies of 287.5, 286.5, 285.7, 284.6 and 284.0 eV, which can be attributed to O-C=O, C=O, C-N, C-C and C-Si bonds. The spectrum of Si 2p shown in Figure S3(C) can be deconvoluted into three peaks located at 103.6, 102.9 and 102.6 eV, which should be attributed to Si-C, Si-O-Si and Si-OH groups. The oxidation state of the Cu in CuBA@$SiO_2$ nanocomposites is shown in FigureS3 (D). The two bands located at 953.8 and 933.8 eV are attributed to Cu $2p_{1/2}$ and Cu $2p_{3/2}$, which consists with the report for Cu in +2 oxidation state [S1].

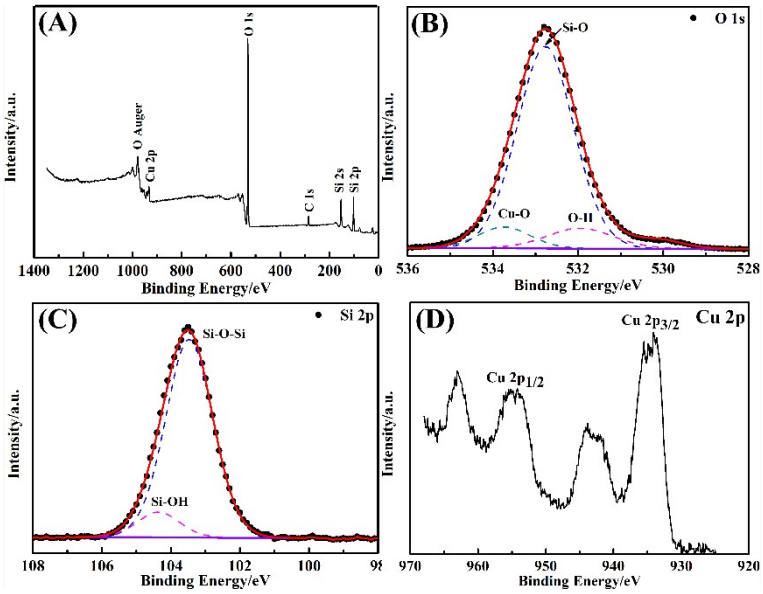


Figure S4 XPS spectra of the obtained CuO@m$SiO_2$ nanocomposites

Figure S4 shows the typical XPS spectra of the obtained CuO@$SiO_2$ naoncomposites. After the thermal treatment, all alkyl chains were decomposed and CuO NPs were in situ generated. The full scanned spectrum shown in Figure S4(A) gives the information of the remnant elements of O, Si and Cu in CuO@$SiO_2$ nanocomposites. Figure S4 (B) shows the spectra of O 1s, which can be deconvoluted into three peaks located at 533.7, 532.7 and 531.9 eV, revealing the Cu-O, Si-O and O-H groups in the obtained CuO@$SiO_2$ naoncomposites. The spectra of Si 2p shown in Figure S4(C) deconvoluted into two peaks located at 104.4 and 103.6 eV can be assigned to Si-OH and Si-O-Si respectively. Figure S4(D) reveals several peaks of Cu 2p after thermal treatment, the main Cu $2p_{3/2}$ peak at 935.4 eV and the corresponding Cu $2p_{1/2}$ peak shifted to 20 eV higher binding energies can be attributed to CuO [S2]. The two satellite peaks in the region of 940-944 eV and 963.3 eV provide more evidence for the formation of CuO NPs [S3].

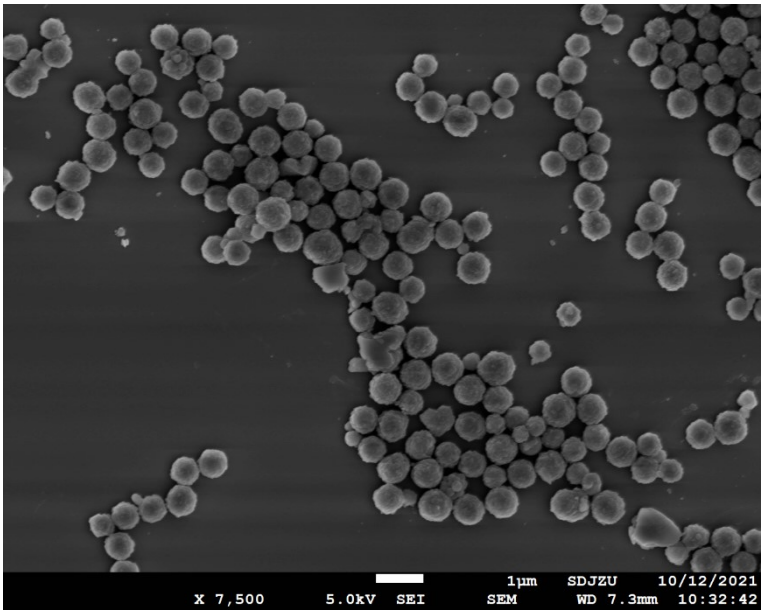


Figure S5 SEM image of $CuO@mSiO_2$ nanocomposites

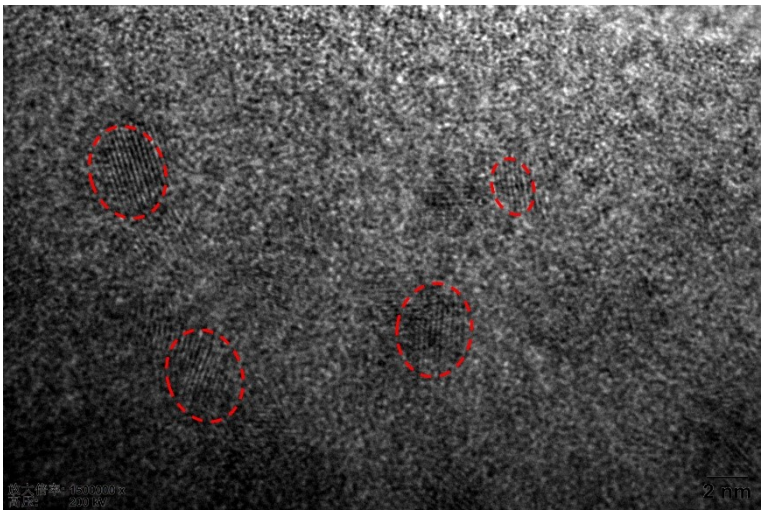


Figure S6 HRTEM image of $CuO@mSiO_2$ nanocomposites

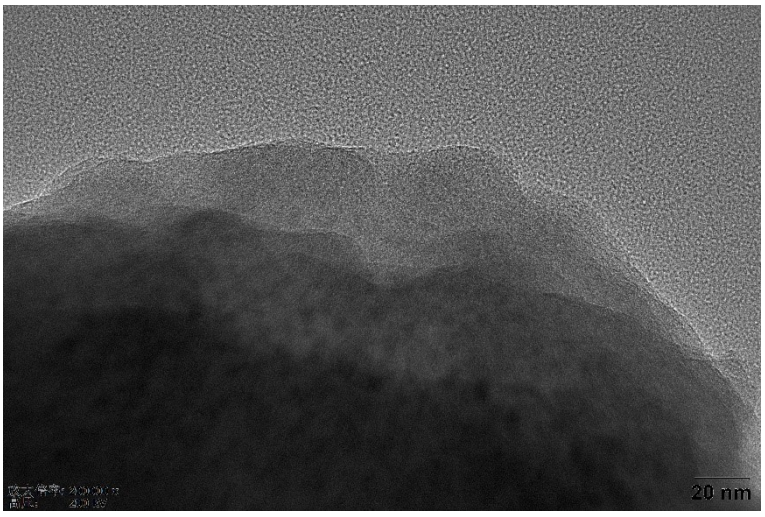


Figure S7 TEM image of $CuO@mSiO_2$ nanocomposites

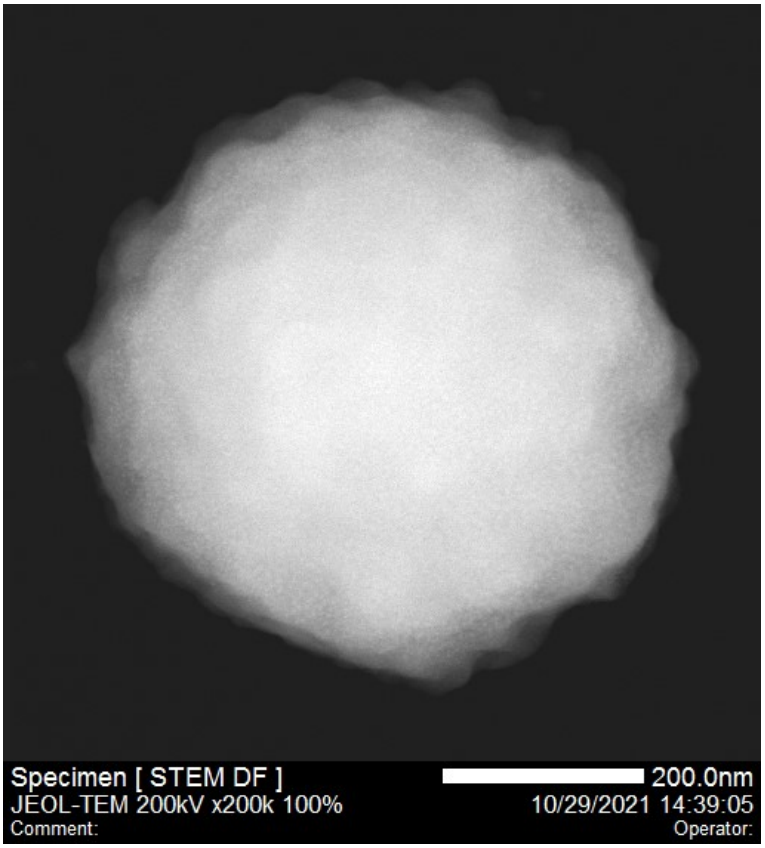


Figure S8 HADDF image of CuO@mSiO$_2$ nanocomposites

CuBA was covalently bonded with APTES, resulting in forming a multifunctional molecule that not only contains silicon alkoxides but also contains copper ions. Thus when the sol-gel process occurred, organic copper salt was introduced into Si-O-Si networks. Figure S7 and Figure S8 can provide the evidence that CuO NPs are uniformly dispersed into silica matrix.

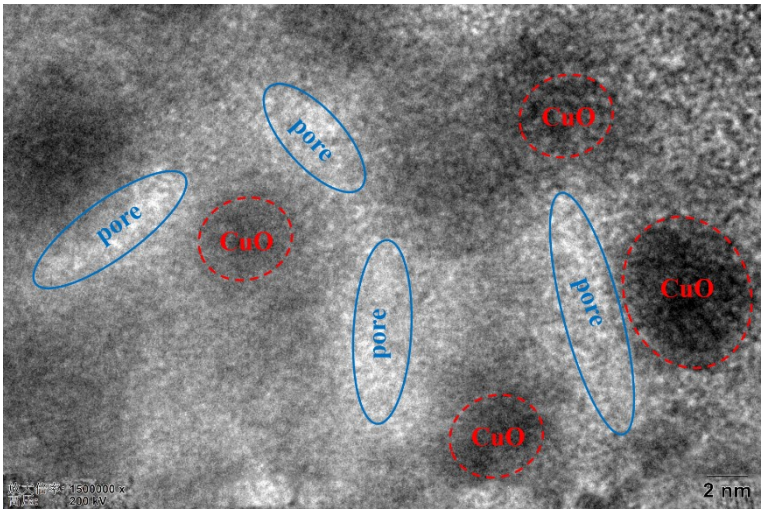


Figure S9 magnified TEM image of CuO@mSiO$_2$ nanocomposites

Table S1 Comparison of catalytic performances of different catalysts from the literature

| Entry | Catalyst | $K$ ($s^{-1}$) | $K'$ ($s^{-1}$ $g^{-1}$) | Ref. |
|---|---|---|---|---|
| 1 | Pd/ZnO@Zn | $4.63\times10^{-3}$ | 76.6 | S4 |
| 2 | Pd/carbon nanotube | $10.5\times10^{-3}$ | 124.65 | S5 |
| 3 | PdAu/graphene | $6.5\times10^{-3}$ | 130 | S6 |
| 4 | Pd/MWCNT | $1.9\times10^{-3}$ | 114 | S7 |
| 5 | Met-AgNP | $1.2\times10^{-3}$ | 112.27 | S8 |
| 6 | CNFs@Au | $5.4\times10^{-3}$ | 54.20 | S9 |
| 7 | CuO@m$SiO_2$ | $2.23\times10^{-3}$ | 174.4 | This work |

$K$, the kinetic rate constant was calculated from the ralationships between $\ln(C_t/C_0)$ and reaction time.

$K'$, the catalytic activity factor was calculated by using eqn $K'= K/M_{metal}$

**Refences**


[S1] T L Freeman and S D Evans, Multilayers of ω-mercaptoalkanoic acids containing a polar aromatic group: characterization of films, *Thin Solid Films,* 1994, **244**, 784-788.

[S2] F Klein, R Pinedo, P Hering, A Polity, J Janek and P Adelhelm, Reaction Mechanism and Surface Film Formation of Conversion Materials for Lithium- and Sodium-Ion Batteries: An XPS Case Study on Sputtered Copper Oxide (CuO) Thin Film Model Electrodes, *J. Phys. Chem. C,* 2016, **120**, 1400-1414.

[S3] J Zhang, J Liu, Q Peng, X Wang and Y Li, Nearly Monodisperse $Cu_2O$ and CuO Nanospheres: Preparation and Applications for Sensitive Gas Sensors, *Chem. Mater*, 2006, **18**, 867–871.

[S4] Q. Y. Hu, X. W. Liu, L. Tang, D. W. Min, T. C. Shi, W. Zhang, Pd–ZnO nanowire arrays as recyclable catalysts for 4-nitrophenol reduction and Suzuki coupling reactions, *RSC Adv*, 2017, **7**, 7964-7972

[S5] X. M. Gu, W. Qi, X. Z. Xu, Z. H. Sun, L. Y. Zhang, W. Liu, X. L. Pan, D. S. Su, Covalently functionalized carbon nanotube supported Pd nanoparticles for catalytic reduction of 4-nitrophenol, *Nanoscale*, 2014, **6**, 6609-6616.

[S6] C. H. Liu, R. H. Liu, Q. J. Sun, J. B. Chang, X. Gao, Y. Liu, S. T. Lee, Z. H. Kang, S. D. Wang, Controlled synthesis and synergistic effects of graphene-supported PdAu bimetallic nanoparticles with tunable catalytic properties, *Nanoscale*, 2015, **7**, 6356-6362.

[S7] C. H. Liu, J. Liu, Y. Y. Zhou, X. L. Cai, Y. Lu, X. Gao, S. D. Wang, Small and uniform Pd monometallic/bimetallic nanoparticles decorated on multi-walled carbon nanotubes for efficient reduction of 4-nitrophenol, *Carbon*, 2015, **94**, 295–300.

[S8] A. Chandra, M. Singh, Biosynthesis of amino acid functionalized silver nanoparticles for potential catalytic and oxygen sensing applications, *Inorg. Chem. Front.*, 2018, **5**, 233-257.

[S9] P Zhang, C Shao, X Li, M Zhang, X Zhang, C Su, N Lu, K Wang, Y Liu, Phys. An electron-rich free-standing carbon@Au core–shell nanofiber network as a highly active and recyclable catalyst for the reduction of 4-nitrophenol, *Chem. Chem. Phys.*, 2013, **15**, 10453–10458.